

Three-tone coherent microwave electromechanical measurement of a superfluid Helmholtz resonator

Spence, S.; Varga, E.; Potts, C. A.; Davis, J. P.

DOI

[10.1063/5.0165488](https://doi.org/10.1063/5.0165488)

Publication date

2023

Document Version

Final published version

Published in

Applied Physics Letters

Citation (APA)

Spence, S., Varga, E., Potts, C. A., & Davis, J. P. (2023). Three-tone coherent microwave electromechanical measurement of a superfluid Helmholtz resonator. *Applied Physics Letters*, 123(11), Article 114001. <https://doi.org/10.1063/5.0165488>

Important note

To cite this publication, please use the final published version (if applicable). Please check the document version above.

Copyright

Other than for strictly personal use, it is not permitted to download, forward or distribute the text or part of it, without the consent of the author(s) and/or copyright holder(s), unless the work is under an open content license such as Creative Commons.

Takedown policy

Please contact us and provide details if you believe this document breaches copyrights. We will remove access to the work immediately and investigate your claim.

Green Open Access added to TU Delft Institutional Repository

'You share, we take care!' - Taverne project

<https://www.openaccess.nl/en/you-share-we-take-care>

Otherwise as indicated in the copyright section: the publisher is the copyright holder of this work and the author uses the Dutch legislation to make this work public.

RESEARCH ARTICLE | SEPTEMBER 11 2023

Three-tone coherent microwave electromechanical measurement of a superfluid Helmholtz resonator

S. Spence   ; E. Varga  ; C. A. Potts  ; J. P. Davis  

 Check for updates

Appl. Phys. Lett. 123, 114001 (2023)

<https://doi.org/10.1063/5.0165488>



View Online



Export Citation

CrossMark

Articles You May Be Interested In

Turbulence in He II Generated by Superflow

AIP Conference Proceedings (September 2006)

Decaying Kolmogorov turbulence in a model of superflow

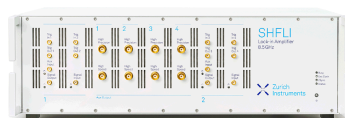
Physics of Fluids (September 1997)

Second-sound studies of coflow and counterflow of superfluid ⁴He in channels

Physics of Fluids (June 2015)

500 kHz or 8.5 GHz? And all the ranges in between.

Lock-in Amplifiers for your periodic signal measurements



Find out more



Three-tone coherent microwave electromechanical measurement of a superfluid Helmholtz resonator

Cite as: Appl. Phys. Lett. **123**, 114001 (2023); doi: [10.1063/5.0165488](https://doi.org/10.1063/5.0165488)

Submitted: 28 June 2023 · Accepted: 23 August 2023 ·

Published Online: 11 September 2023



View Online



Export Citation



CrossMark

S. Spence,^{1,a)}  E. Varga,²  C. A. Potts,³  and J. P. Davis^{1,a)} 

AFFILIATIONS

¹Department of Physics, University of Alberta, Edmonton, Alberta T6G 2E9, Canada

²Faculty of Mathematics and Physics, Charles University, Ke Karlovu 3, 121 16 Prague, Czech Republic

³Kavli Institute of NanoScience, Delft University of Technology, P.O. Box 5046, 2600 GA Delft, Netherlands

^{a)}Authors to whom correspondence should be addressed: stspence@ualberta.ca and jdavis@ualberta.ca

ABSTRACT

We demonstrate electromechanical coupling between a superfluid mechanical mode and a microwave mode formed by a patterned microfluidic chip and a 3D cavity. The electric field of the chip-cavity microwave resonator can be used to both drive and detect the motion of a pure superflow Helmholtz mode, which is dictated by geometric confinement. The coupling is characterized using a coherent measurement technique developed for measuring weak couplings deep in the sideband unresolved regime. The technique is based on two-probe optomechanically induced transparency/amplification using amplitude modulation. Instead of measuring two probe tones separately, they are interfered to retain only a signal coherent with the mechanical motion. With this method, we measure a vacuum electromechanical coupling strength of $g_0 = 2\pi \times 23.3 \mu\text{Hz}$, three orders of magnitude larger than previous superfluid electromechanical experiments.

Published under an exclusive license by AIP Publishing. <https://doi.org/10.1063/5.0165488>

Cavity optomechanics,¹ the coupling of optical and mechanical resonances, is an extremely sensitive scheme for detecting and controlling mechanical motion. Popular optomechanical architectures include vibrating membranes,^{2–5} superconducting drums,^{6–8} phononic crystal cavities,^{9,10} and magnetic spheres,^{11,12} while decidedly more exotic, superfluid helium has been explored as a promising mechanical element for cavity optomechanical and electromechanical experiments—in part due to its large bandgap,^{13,14} low dielectric loss,¹⁵ and ultra-low acoustic loss at millikelvin temperatures.^{16,17} Superfluid helium mechanical resonators have been used to develop gravitational wave detectors^{18,19} and have even been suggested for generating a mechanical qubit²⁰ and for detecting dark matter,²¹ while superfluid optomechanical resonators are allowing new studies of superfluid properties such as novel explorations of vortex dynamics.²² Microfabricated superfluid mechanical resonators—to date lacking the optomechanical component—have also proven to be particularly useful in the study of confined helium, where confinement can dramatically change the physics of the system.^{23,24} Previously, our group has developed microfluidic Helmholtz resonators for this purpose,^{17,25,26} which have been used in ⁴He to discover bi-stable turbulence in 2D superflow²⁷ and reveal surface-dominated finite-size effects at the nanoscale.²⁸

These devices have also been used to search for pair density wave states in superfluid ³He.²⁹ Here, we combine the concepts of microwave cavity electromechanics with microfluidic confinement of superfluid helium-4 within a microfabricated Helmholtz resonator.

In this work, a helium volume is enclosed between two nanofabricated quartz substrates, defining a fourth sound³⁰ (pure superflow) Helmholtz mode inside the microfluidic chip.^{17,25,26} The pressure field of this mode is shown in the inset of Fig. 1. Previously, Varga and Davis³¹ showed the value in electromechanical drive and detection of the Helmholtz mode using kHz-frequency carrier signals in a cavity-less system. Here, we bring the readout into the GHz microwave regime by integrating the chip into a hermetically sealed 3D microwave cavity filled with superfluid ⁴He with on-chip superconducting aluminum electrodes concentrating the cavity's electric field into the Helmholtz basin (Fig. 1), similar to work with SiN membrane chips in 3D microwave cavities.^{2,3} A three-tone coherent drive and measurement technique was developed to observe small mechanical signals and calibrate the optomechanical coupling rate, g_0 , using a strong pump microwave tone, which is amplitude modulated to give two weak probe tone sidebands. The chip-cavity system's effect on the two sidebands is analogous to optomechanically induced transparency and

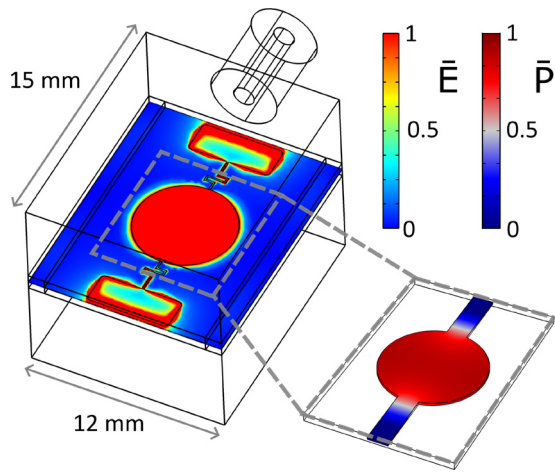


FIG. 1. The chip-cavity system. The outline shows the 3D microwave cavity and pin coupler, while the relative electric field magnitude ($\bar{E} = E(r)/\max[E(r)]$, where $E(r)$ is the electric field amplitude at r of the fundamental chip-cavity microwave mode, concentrated between the central basin capacitive plates and around the antenna, is shown according to the left color bar. Inset: the relative pressure ($\bar{P} = P(r)/\max[P(r)]$, where $P(r)$ is the pressure field amplitude at r of the superfluid Helmholtz mode within the fluid geometry of the chip. Pressure is concentrated in the central basin with relative amplitude according to the right color bar. The channel length has been extended here for visual clarity of the mode shape.

amplification (OMIT/A).³² Demodulating the signal to destructively interfere the two probe tones recovers only the coherent microwave signal containing information about the mechanical motion. This provides a powerful measurement technique in the sideband unresolved regime, especially useful for detecting mechanics in systems with weak opto/electro-mechanical couplings. We use this technique to characterize the chip-cavity electromechanical coupling, measuring a vacuum electromechanical coupling of $g_0 = 2\pi \times 23.3 \mu\text{Hz}$.

As mentioned above, the experimental system consists of a superfluid Helmholtz resonator, similar to Refs. 17, 27, and 31, but now incorporated into a hermetic 3D microwave cavity. The etched Helmholtz geometry is a wide flat circular basin, 7 mm in diameter and $1.01 \mu\text{m}$ deep, connected by two 1.6 mm wide and 1.6 mm long channels to the surrounding helium bath. Electrodes of 50 nm thick aluminum are deposited into the etched regions: a 6 mm diameter circle at the center of the basin connects to a meandering $100 \mu\text{m}$ -wide lead (in one channel) that terminates in a $5 \times 2 \text{ mm}^2$ square antenna. After fabrication, the wafer is diced into identical top and bottom chips, which are room-temperature direct wafer bonded^{33,34} such that the basins align and the antennas are on opposite sides of the basin (as shown in Fig. 1). The combined basins form a single volume with aluminum top and bottom electrodes, turning the combined basin into a parallel plate capacitor, with an antenna connected to each plate—providing capacitive coupling to the 3D cavity mode. (More detailed fabrication notes can be found in Ref. 17.)

The Helmholtz mode is an acoustic resonance of the superfluid moving back and forth in the channel, driven by pressure fluctuations in the central basin (shown in the inset of Fig. 1). The mode can be described as a mass-spring system²⁷ with effective mass $m_{\text{eff}} = 2wD\rho_s$,

where w , l , and D are the channel width, length, and depth, respectively; and ρ_s is the superfluid density. The resulting mode frequency is then³¹

$$\Omega_m = \sqrt{\frac{k_{\text{eff}}}{m_{\text{eff}}}} = \sqrt{\frac{2wD\rho_s}{l\rho} \frac{k_p}{4A^2(1+\Sigma)}}, \quad (1)$$

with k_{eff} being the effective spring constant, k_p being the effective stiffness of the mean deflection of the basin walls, $A = \pi R^2$ being the area of the basin, and $\Sigma = \chi_B D k_p / (4A)$, where χ_B is the bulk compressibility of helium. Here, the effective spring constant of the mode is significantly softened by the flexing of the substrate when compared to the compressibility-only case. The flexing of the substrate changes the distance between the capacitive plates above and below the basin, the origin of the electromechanical coupling for this system, which is slightly suppressed by electrostriction due to the compression of the helium.^{35,36} Considering both of these factors, the change in basin capacitance C_{bas} can be written in terms of the displacement of the fluid in the channels y , as³¹

$$\frac{dC_{\text{bas}}}{dy} = \bar{C}_{\text{bas}} \frac{2w\rho_s}{A\rho} \left(1 - \frac{\varepsilon - 1}{\varepsilon} \Sigma\right) \frac{1}{1 + \Sigma}, \quad (2)$$

where \bar{C}_{bas} is the undeformed basin capacitance and ε is the dielectric constant of liquid helium.

The Helmholtz chip is placed at the center of a rectangular 3D microwave cavity,³⁷ and the 3D cavity mode is capacitively coupled to the basin capacitor via the on-chip antenna,³⁸ effectively concentrating the electric field of the fundamental chip-cavity mode into the basin, as shown in Fig. 1. The lumped element RLC representation of the chip-cavity system is shown in Fig. 2(a), and Fig. 2(b) shows a typical S_{21} single port bi-directional (reflection) measurement of the microwave resonance at 600 mK with the cavity filled with superfluid helium-4 close to saturated vapor pressure (SVP). Microwave circuit schematics can be found in the supplementary material. From this measurement, the resonant frequency is found to be $\omega_c = 2\pi \times 2.28 \text{ GHz}$ with total cavity loss rate $\kappa = 2\pi \times 1.76 \text{ MHz}$ and external coupling rate $\kappa_{\text{in}} = 2\pi \times 128 \text{ kHz}$, meaning the system is significantly undercoupled.³⁹

The vacuum electromechanical coupling strength $g_0 = Gx_{\text{zpf}}$, with $G = -\partial\omega_c/\partial x$, can be considered as the shift in cavity resonance due to the zero point motion of the mechanical oscillator. For the Helmholtz chip-cavity system, this can be written as

$$g_0 = -\delta y_{\text{zpf}} \frac{\partial\omega_c}{\partial y} = -\delta y_{\text{zpf}} \frac{\partial\omega_c}{\partial C} \frac{\partial C}{\partial y}, \quad (3)$$

where δy_{zpf} is the zero point motion of the superfluid in the channels and C is the total capacitance of the chip-cavity microwave mode given by $\omega_c = 1/\sqrt{LC}$. Using $\delta y_{\text{zpf}} = \sqrt{\hbar/2m_{\text{eff}}\Omega_m}$, Eq. (2), and that the temperature is cold enough for $\rho_s \approx \rho$, g_0 can be expressed for this electromechanical coupling scheme as

$$g_0 \simeq \alpha\omega_c \sqrt{\frac{\hbar}{2m_{\text{eff}}\Omega_m}} \frac{w}{A} \left(1 - \frac{\varepsilon - 1}{\varepsilon} \Sigma\right) \frac{1}{1 + \Sigma}. \quad (4)$$

Here, α is the proportion of the microwave mode's total electric field energy within the basin capacitor; for this work, $\alpha \approx 0.005$ is calculated via finite element method (FEM) simulations. Equation (4) gives a method for estimating the g_0 of a fabricated device. Only Ω_m and k_p

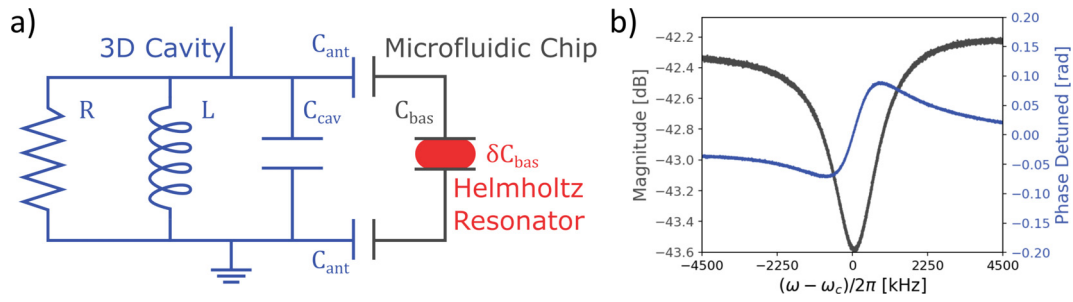


FIG. 2. Left: An RLC representation of the chip-cavity system, showing the 3D microwave cavity in blue, the microfluidic chip in black, and the superfluid Helmholtz mode in red. The resistance, inductance, and capacitance of the bare 3D cavity are represented by R , L , and C_{cav} , respectively. The capacitance between the on-chip antenna and the 3D cavity is represented by the two C_{ant} and the on-chip Helmholtz basin capacitance by C_{bas} . Right: A typical reflection measurement (via a directional coupler) of the cavity at 600 mK when filled with superfluid ^4He . The magnitude is shown in gray, while the detuned phase is shown in blue. Frequency has been detuned around the microwave cavity frequency $\omega_c = 2\pi \times 2.28$ GHz.

are unknown, yet Ω_m can be estimated using Eq. (1) while $k_p = 9.45 \times 10^6 \text{ N m}^{-1}$ is measured via capacitance change with a DC bias, as in Ref. 17. Using these values an estimate of $g_0 \approx 2\pi \times 1.1 \mu\text{Hz}$ is obtained; although lower than the value found later in this work, this discrepancy is likely due to inaccuracy in α .

We began by observing electromechanical coupling using a calibrated homodyne measurement:^{36,40,41} sending a tone at the microwave resonance’s maximum gradient, demodulating the returned signal with a tone of the same frequency, measuring noise in the time domain, and considering the power spectral density of fluctuations near the mechanical frequency Ω_m (circuit shown in the supplementary material). Reflection via a directional coupler was measured as the return signal. The mechanical spectrum was found using an amplitude-sensitive scheme, giving a Helmholtz mode frequency of $\Omega_m = 2\pi \times 1394.7$ Hz. The homodyne phase-lock was achieved by applying a 10 kHz phase modulation to the signal on the cavity arm of the circuit and then minimizing the 10 kHz signal after down-mixing by varying the LO phase. Phase-sensitive measurement was also possible by instead sending the microwave tone on resonance and using the 10 kHz amplitude modulation to phase-lock.

Despite homodyne measurement enabling detection of the mechanical spectrum, the signal is weak with a small signal-to-noise ratio near the mechanical resonance frequency, mainly due to low electromechanical coupling strength and undercoupled microwave readout, even after more than 450 averages. Moreover, determination of g_0 was not possible due to uncertainty in the effective temperature of the Helmholtz mode since vibrations from the cryocooler drove the superfluid motion in the present experiment.

A coherent measurement scheme can be used to precisely determine the electromechanical coupling rate, g_0 . The scheme in this work is based on OMIT/A,^{32,42–44} an interference effect where beating between two optical tones causes coherent oscillation of the mechanics via radiation pressure when the two tones are separated in frequency by the mechanical resonance. The oscillation of the mechanics, in turn, scatters photons from the stronger driving “pump” tone to the weak “probe” tone frequency, where they then destructively (constructively) interfere with the probe tone in the case of OMIT (OMIA). In the microwave regime, the equivalent effect is often called electromechanically induced transparency/amplification (EMIT/A).⁴⁵ For the Helmholtz devices, mechanical motion is driven via modulation of the

electrostatic force between the two capacitive basin plates, proportional to voltage squared. Typically, OMIT/A is used for sideband resolved systems ($\kappa \ll \Omega_m$) with stronger optomechanical coupling strengths compared to this work. To overcome these limitations, a “two-probe” measurement scheme is used here. The two probe tones are produced by amplitude modulation of the pump tone, inspired by the work of Kashkanova *et al.*⁴⁶ and adapted from optics to the microwave regime. For this work, modulation of a microwave signal allows straightforward resolution of a mHz mechanical linewidth on a GHz signal and, for kHz mechanics deep into the sideband unresolved regime, enables a unique measurement scheme where the probe tones are canceled to recover only a coherent electromechanical signal, which would not be visible otherwise.

Figure 3 shows a diagram of the coherent measurement scheme in this work. In Fig. 3(a), a strong microwave pump tone with frequency ω_d is sent into the cavity, at some detuning Δ from the cavity resonance ω_c , such that $\Delta = \omega_d - \omega_c$. This pump tone is amplitude modulated with frequency Ω_p to produce the two weak probe signals at $\omega_p^\pm = \omega_d \pm \Omega_p$. The signal incident at the cavity port can then be written as $s_{in} = \bar{s}_{in} + \delta s_{in}$, where the weak probes provide δs_{in} , which in a frame rotating at ω_d can be written as

$$\delta s_{in} = s_p (e^{-i\Omega_p t} + e^{+i\Omega_p t})/2. \quad (5)$$

Here, $s_p/2$ is the amplitude of the probe signals. Sweeping Ω_p across the mechanical frequency Ω_m , equivalent to sweeping the probe and pump separation, causes the EMIT/A effect close to Ω_m for the upper and lower sidebands, respectively, shown in the inset of Fig. 3(a). Following the full derivation in the supplementary material, the intracavity field amplitude at the two probe frequencies ω_p^\pm can be written as

$$A^\pm(\Omega_p) = \frac{\chi_\pm \sqrt{\kappa_{in}} s_p}{2} \left(1 \mp \frac{g(g\chi_\mp^* + g^*\chi_\pm)}{\Gamma_m/2 \mp i\delta \pm i\Sigma(\pm\Omega_p)} \right), \quad (6)$$

where Γ_m is the mechanical linewidth, $\delta = \Omega_p - \Omega_m$ is the detuning of the pump-probe separation from the mechanical frequency, g is the multiphoton coupling defined as

$$g = g_0 \frac{\sqrt{\kappa_{in}} \bar{s}_{in}}{-i\Delta + \kappa/2}, \quad (7)$$

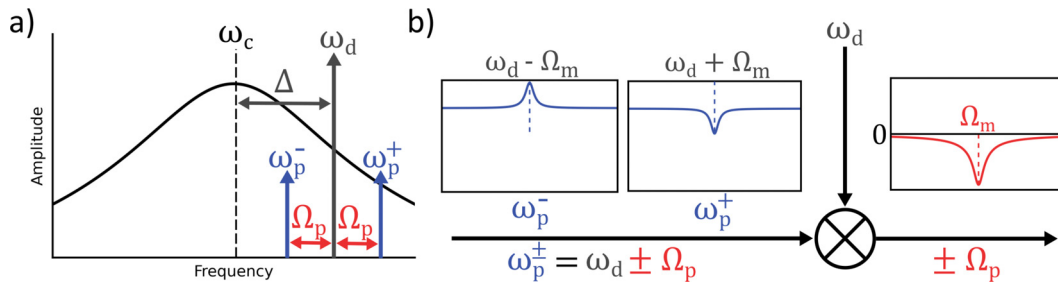


FIG. 3. Diagram of the three-tone coherent measurement scheme. (a) Frequency space diagram of the three tones relative to the microwave resonance ω_c . Showing the pump tone ω_d at detuning Δ from the cavity resonance, along with the two probe tones ω_p^\pm created via amplitude modulation of the pump tone with frequency (separation) Ω_p . The cavity resonance line shape has been reduced for clarity. (b) Diagram of the two probe tones before (left—blue) and after (right—red) demodulation. The left side shows the response at the probe tones ω_p^\pm as the modulation frequency Ω_p is swept across the mechanical frequency Ω_m , showing the EMIT/A response for the upper and lower sidebands, respectively. The flat background is due to being deep into the sideband unresolved regime $\kappa \gg \Omega_m$. The right side shows the measured signal at relative phase $\phi = 0$, after demodulating the two probe tones with the pump frequency ω_d . This down mixes the probe signals to frequency $\pm\Omega_p$, where the two probe tones destructively interfere, leaving only the combined EMIT/A signal with a peak at Ω_m .

χ_\pm is the cavity susceptibility at ω_p^\pm ,

$$\chi_\pm = \frac{1}{-i(\Delta \pm \Omega_p) + \kappa/2}, \quad (8)$$

and the electromechanical self-energy $\Sigma(\Omega_p)$ is defined as

$$i\Sigma(\Omega_p) = |g|^2(\chi_+ - \chi_-^*). \quad (9)$$

When measuring in a bi-directional single port scheme (reflection via a circulator/directional coupler), $-\sqrt{\kappa_{in}}A^\pm$ is effectively the modification of the reflected probe tones due to the cavity electromechanical system. Demodulating this reflected signal at ω_d and a relative phase of $\phi = 0$ will give a signal at Ω_p with amplitude proportional to the upper probe minus the lower probe, canceling out the probe tone backgrounds and recovering only the coherent effect, shown in Fig. 3(b). Measuring this signal at Ω_p using a lock-in amplifier will give a signal

$$X + iY = \frac{-iK_T g_0^2 \kappa_{in}^2 s_p (\kappa^2/4 - \Delta^2) P_{in}}{\sqrt{2}(\Gamma_m/2 + i\delta) (\kappa^2/4 + \Delta^2)^3 \hbar \omega_d}, \quad (10)$$

where K_T is the transfer function of the circuit post reflection from the cavity and P_{in} is the total power incident on the cavity port. A full derivation of $X + iY$ can be found in the supplementary material. Figure 4(b) shows a measurement of the Y quadrature, fit to Eq. (10), showing an improvement of fitting accuracy and signal-to-noise near resonance, compared to the homodyne measurement of noise amplitude spectral density in Fig. 4(a). From the coherent measurement fit, the mechanical frequency and linewidth are found to be $\Omega_m = 2\pi \times 1394.7$ Hz and $\Gamma_m = 2\pi \times 0.106$ Hz. Although it may instead be possible to cancel the probe tones using an additional source, with the current method far into the sideband unresolved regime ($\kappa \gg \Omega_m$), the two probe tones effectively travel the same path, canceling near perfectly and accounting for any frequency, phase, or amplitude noise. Using the three-tone method, the background signal at Ω_m was reduced by three to four orders of magnitude, allowing a measurement of the mechanics that would not normally be possible with EMIT/A.

The circuit transfer function K_T in Eq. (10) can be calibrated to allow determination of g_0 using a measurement of $R = |X + iY|$ with $\phi = \pi/2$ to give a signal proportional to the combined probe tone

amplitudes $R_{cal} = K_T s_p / 2\sqrt{2}$ (further details in the supplementary material). Using this calibration, g_0 can be written as

$$g_0 = \frac{\sqrt{\hbar \omega_d}}{2\kappa_{in} \sqrt{P_{in}}} \sqrt{\frac{\Gamma_m (\kappa^2/4 + \Delta^2)^3 R_{\delta=0}}{(\kappa^2/4 - \Delta^2) R_{cal}}}. \quad (11)$$

Here, $R_{\delta=0}$ is the measured signal amplitude at $\Omega_p = \Omega_m$ when the probe tones cancel, either directly from the peak signal or from fitting to Eq. (10). Using this methodology, the vacuum electromechanical coupling strength was calculated as $g_0 = 2\pi \times 23.3_{-4.8}^{+6.0}$ μ Hz with determination of P_{in} providing the dominant error. This g_0 is in the weak coupling limit of electromechanics,¹ but a three order of magnitude increase when compared to a bulk superfluid-microwave coupling,⁴⁷ and even higher than the potential g_0 of current bulk systems mediated by a membrane.¹⁹ While the corresponding single-photon cooperativity $C_0 = 1.2 \times 10^{-14}$ is one of the lowest recorded¹ and will need to be improved in subsequent experiments, this demonstrates the sensitivity of the three-tone coherent measurement scheme.

In conclusion, the superfluid microwave electromechanical coupling was measured for a micromechanical system using a microfluidic Helmholtz resonator inside a 3D microwave cavity. The mechanical motion was detected using a homodyne noise measurement scheme; however, thermomechanical calibration was not possible due to strong cryocooler vibrations. To measure an electromechanical system with weak coupling, deep in the sideband unresolved regime, a coherent measurement scheme was developed, inspired by OMIT³² and specifically the work of Kashkanova *et al.*⁴⁶ The scheme uses amplitude modulation of a strong pump tone to create probe sidebands, which experience coherent EMIT/A. The two probe tones are then canceled to recover only signal coherent with the mechanics, allowing an electromechanical calibration of the coupling strength g_0 , even when the effective mode temperature cannot be determined.

The coherent measurement scheme provides a powerful tool for measuring electro/optomechanical systems deep into the sideband unresolved regime. Moreover, integrating a superfluid Helmholtz device into a microwave cavity provides a platform for superfluid microwave electromechanics. With three orders of magnitude improvement to g_0 over initial bulk superfluid electromechanical systems,³⁵ the microwave Helmholtz design shows promise as a sensitive

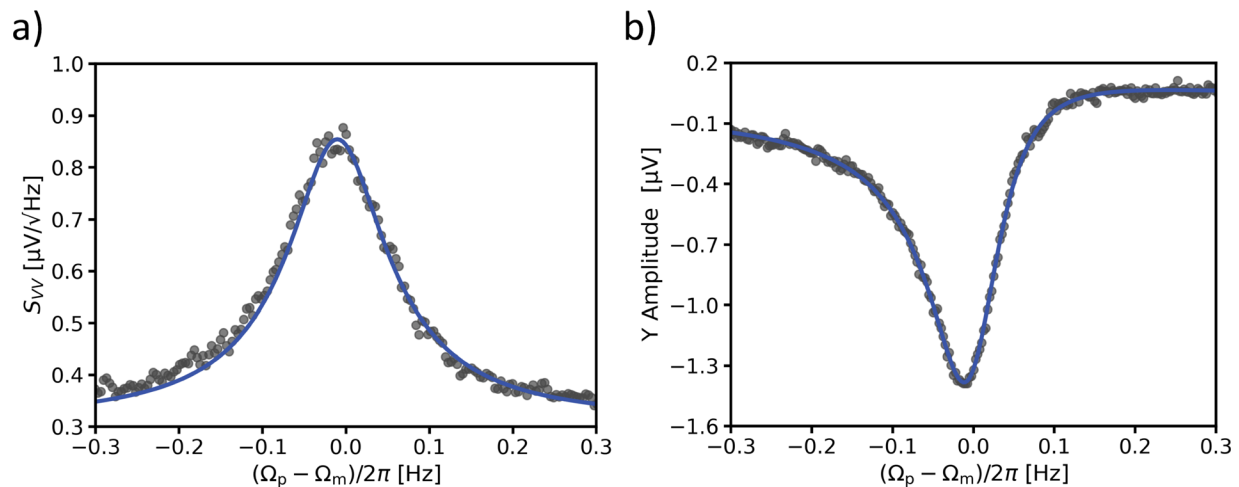


FIG. 4. (a) Homodyne noise measurement: plotting noise amplitude spectral density of the Helmholtz mode, as driven by the environmental noise of the cryocooler. The average of 453 acquisitions is shown. (b) Coherent three-tone measurement (EMIT/A): plotting the amplitude measured at the lock-in vs amplitude modulation frequency, detuned around the mechanical resonance Ω_m , a constant background has been subtracted. The average of 37 acquisitions is shown. The slight asymmetry of the EMIT/A response is due to a small phase offset in the complex Lorentzian response shape.

method for measuring the properties of superfluid helium. The sensitivity of this proof of concept can be improved by orders of magnitude in many areas: confinement could decrease Γ_m while increasing g_0 (possibly with a phononic crystal^{20,48}), larger antennas or galvanic bonding would increase α ,³ low mK dilution temperatures would decrease superfluid and microwave dissipation, a superconducting microwave cavity could also decrease dissipation, and a stronger coupling into the cavity ($\kappa_{in} \approx \kappa/2$) would greatly improve signal strength for any given cavity field. The improved system may be useful for studying non-equilibrium thermodynamics⁴⁹ or even vector dark matter.⁵⁰

See the supplementary material for derivation of the three-tone coherent measurement equations and calibration of vacuum electro-mechanical coupling strength. It also includes microwave circuit diagrams and measurement descriptions for both the three-tone and homodyne methods along with photos of the experimental cell.

The authors acknowledge that the land on which this work was performed is in Treaty Six Territory, the traditional territories of many First Nations, Métis, and Inuit in Alberta. They acknowledge support from the University of Alberta; the Natural Sciences and Engineering Research Council, Canada (Grant Nos. RGPIN-2022-03078 and CREATE-495446-17); the NSERC Alberta Innovates Advance Program (ALLRP-568609-21); and the Government of Canada through the NRC Quantum Sensors Program.

AUTHOR DECLARATIONS

Conflict of Interest

The authors have no conflicts to disclose.

Author Contributions

Sebastian Spence: Conceptualization (supporting); Formal analysis (lead); Methodology (equal); Software (lead); Writing – original draft

(lead); Writing – review & editing (lead). **Emil Varga:** Conceptualization (lead); Formal analysis (supporting); Methodology (equal); Supervision (supporting); Writing – original draft (supporting); Writing – review & editing (supporting). **Clinton A. Potts:** Formal analysis (supporting); Software (supporting); Writing – original draft (supporting); Writing – review & editing (supporting). **John P. Davis:** Conceptualization (supporting); Funding acquisition (lead); Supervision (lead); Writing – original draft (supporting); Writing – review & editing (supporting).

DATA AVAILABILITY

The data that support the findings of this study are available from the corresponding authors upon reasonable request.

REFERENCES

- 1M. Aspelmeyer, T. J. Kippenberg, and F. Marquardt, *Rev. Mod. Phys.* **86**, 1391 (2014).
- 2M. Yuan, V. Singh, Y. M. Blanter, and G. A. Steele, *Nat. Commun.* **6**, 8491 (2015).
- 3A. Noguchi, R. Yamazaki, M. Ataka, H. Fujita, Y. Tabuchi, T. Ishikawa, K. Usami, and Y. Nakamura, *New J. Phys.* **18**, 103036 (2016).
- 4A. Pearson, K. Khosla, M. Mergenthaler, G. A. D. Briggs, E. Laird, and N. Ares, *Sci. Rep.* **10**, 1654 (2020).
- 5J. M. Pate, M. Goryachev, R. Y. Chiao, J. E. Sharping, and M. E. Tobar, *Nat. Phys.* **16**, 1117–1122 (2020).
- 6J. D. Teufel, T. Donner, D. Li, J. W. Harlow, M. Allman, K. Cicak, A. J. Sirois, J. D. Whittaker, K. W. Lehnert, and R. W. Simmonds, *Nature* **475**, 359–363 (2011).
- 7S. Kotler, G. A. Peterson, E. Shojaei, F. Lecocq, K. Cicak, A. Kwiatkowski, S. Geller, S. Glancy, E. Knill, R. W. Simmonds *et al.*, *Science* **372**, 622–625 (2021).
- 8D. Cattiaux, I. Golokolenov, S. Kumar, M. Sillanpää, L. Mercier de Lépinay, R. Gazizulin, X. Zhou, A. Armour, O. Bourgeois, A. Fefferman, and E. Collin, *Nat. Commun.* **12**, 6182 (2021).
- 9P. Arrangoiz-Arriola, E. A. Wollack, M. Pechal, J. D. Witmer, J. T. Hill, and A. H. Safavi-Naeini, *Phys. Rev. X* **8**, 031007 (2018).
- 10E. Serra, A. Borrielli, F. Marin, F. Marino, N. Malossi, B. Morana, P. Piergentili, G. A. Prodi, P. M. Sarro, P. Vezio *et al.*, *J. Appl. Phys.* **130**, 064503 (2021).

- ¹¹X. Zhang, C.-L. Zou, L. Jiang, and H. X. Tang, *Sci. Adv.* **2**, e1501286 (2016).
- ¹²C. A. Potts, E. Varga, V. A. Bittencourt, S. V. Kusminskiy, and J. P. Davis, *Phys. Rev. X* **11**, 031053 (2021).
- ¹³W. I. Glaberson and W. W. Johnson, *J. Low Temp. Phys.* **20**, 313–338 (1975).
- ¹⁴D. Z. Kandula, C. Gohle, T. J. Pinkert, W. Ubachs, and K. S. Eikema, *Phys. Rev. Lett.* **105**, 063001 (2010).
- ¹⁵W. Hartung, J. Bierwagen, S. Bricker, C. Compton, T. Grimm, M. Johnson, D. Meidlinger, D. Pendell, J. Popielarski, L. Saxton, and R. C. York, *Vacuum* **10**, 755–757 (2006).
- ¹⁶L. De Lorenzo and K. Schwab, *New J. Phys.* **16**, 113020 (2014).
- ¹⁷F. Souris, X. Rojas, P. H. Kim, and J. P. Davis, *Phys. Rev. Appl.* **7**, 044008 (2017).
- ¹⁸S. Singh, L. De Lorenzo, I. Pikovski, and K. Schwab, *New J. Phys.* **19**, 073023 (2017).
- ¹⁹V. Vadakkumbatt, M. Hirschel, J. Manley, T. Clark, S. Singh, and J. Davis, *Phys. Rev. D* **104**, 082001 (2021).
- ²⁰Y. L. Sfindla, C. G. Baker, G. I. Harris, L. Tian, R. A. Harrison, and W. P. Bowen, *npj Quantum Inf.* **7**, 62 (2021).
- ²¹J. Manley, D. J. Wilson, R. Stump, D. Grin, and S. Singh, *Phys. Rev. Lett.* **124**, 151301 (2020).
- ²²Y. P. Sachkou, C. G. Baker, G. I. Harris, O. R. Stockdale, S. Forstner, M. T. Reeves, X. He, D. L. McAuslan, A. S. Bradley, M. J. Davis, and W. P. Bowen, *Science* **366**, 1480–1485 (2019).
- ²³L. Levitin, R. Bennett, A. Casey, B. Cowan, J. Saunders, D. Drung, T. Schurig, and J. Parpia, *Science* **340**, 841–844 (2013).
- ²⁴J. Perron, M. Kimball, and F. Gasparini, *Rep. Prog. Phys.* **82**, 114501 (2019).
- ²⁵A. Duh, A. Suhel, B. Hauer, R. Saeedi, P. Kim, T. Biswas, and J. Davis, *J. Low Temp. Phys.* **168**, 31–39 (2012).
- ²⁶X. Rojas and J. Davis, *Phys. Rev. B* **91**, 024503 (2015).
- ²⁷E. Varga, V. Vadakkumbatt, A. Shook, P. Kim, and J. Davis, *Phys. Rev. Lett.* **125**, 025301 (2020).
- ²⁸E. Varga, C. Undershute, and J. Davis, *Phys. Rev. Lett.* **129**, 145301 (2022).
- ²⁹A. Shook, V. Vadakkumbatt, P. S. Yapa, C. Doolin, R. Boyack, P. Kim, G. Popowich, F. Souris, H. Christani, J. Maciejko, and J. P. Davis, *Phys. Rev. Lett.* **124**, 015301 (2020).
- ³⁰D. R. Tilley and J. Tilley, *Superfluidity and Superconductivity* (Routledge, 2019).
- ³¹E. Varga and J. P. Davis, *New J. Phys.* **23**, 113041 (2021).
- ³²S. Weis, R. Rivière, S. Deléglise, E. Gavartin, O. Arcizet, A. Schliesser, and T. J. Kippenberg, *Science* **330**, 1520 (2010).
- ³³Q.-Y. Tong, G. Cha, R. Gafiteanu, and U. Gosele, *J. Microelectromech. Syst.* **3**, 29–35 (1994).
- ³⁴T. Plach, K. Hingerl, S. Tollabimazraehno, G. Hesser, V. Dragoi, and M. Wimplinger, *J. Appl. Phys.* **113**, 094905 (2013).
- ³⁵L. A. De Lorenzo, “Optomechanics with superfluid helium-4,” Ph.D. thesis (California Institute of Technology, 2016).
- ³⁶S. Spence, “Superfluid optomechanics with nanofluidic geometries,” Ph.D. thesis (Royal Holloway, University of London, 2022).
- ³⁷L. A. De Lorenzo, *Microwave Engineering* (John Wiley & Sons, 2011).
- ³⁸D. I. Schuster, “Circuit quantum electrodynamics,” Ph.D. thesis (Yale University, 2007).
- ³⁹D. Rieger, S. Günzler, M. Spiecker, A. Nambisan, W. Wernsdorfer, and I. Pop, *arXiv:2209.03036* (2022).
- ⁴⁰M. Gorodetsky, A. Schliesser, G. Anetsberger, S. Deleglise, and T. J. Kippenberg, *Opt. Express* **18**, 23236 (2010).
- ⁴¹S. Kumar, S. Spence, S. Perrett, Z. Tahir, A. Singh, C. Qi, S. Perez Vizan, and X. Rojas, *J. Appl. Phys.* **133**, 094501 (2023).
- ⁴²G. S. Agarwal and S. Huang, *Phys. Rev. A* **81**, 041803 (2010).
- ⁴³A. H. Safavi-Naeini, T. M. Alegre, J. Chan, M. Eichenfield, M. Winger, Q. Lin, J. T. Hill, D. E. Chang, and O. Painter, *Nature* **472**, 69–73 (2011).
- ⁴⁴A. Kashkanova, A. Shkarin, C. Brown, N. Flowers-Jacobs, L. Childress, S. Hoch, L. Hohmann, K. Ott, J. Reichel, and J. Harris, *Nat. Phys.* **13**, 74–79 (2017).
- ⁴⁵X. Zhou, F. Hocke, A. Schliesser, A. Marx, H. Huebl, R. Gross, and T. J. Kippenberg, *Nat. Phys.* **9**, 179–184 (2013).
- ⁴⁶A. Kashkanova, A. Shkarin, C. Brown, N. Flowers-Jacobs, L. Childress, S. Hoch, L. Hohmann, K. Ott, J. Reichel, and J. Harris, *J. Opt.* **19**, 034001 (2017).
- ⁴⁷L. De Lorenzo and K. Schwab, *J. Low Temp. Phys.* **186**, 233–240 (2017).
- ⁴⁸S. Spence, Z. Koong, S. Horsley, and X. Rojas, *Phys. Rev. Appl.* **15**, 034090 (2021).
- ⁴⁹D. Awschalom and K. Schwarz, *Phys. Rev. Lett.* **52**, 49 (1984).
- ⁵⁰J. Manley, M. D. Chowdhury, D. Grin, S. Singh, and D. J. Wilson, *Phys. Rev. Lett.* **126**, 061301 (2021).